Available online at www.sciencedirect.com
ScienceDirect
Polymer 48 (2007) 652–663
polymer
www.elsevier.com/locate/polymer

Synthesis, molecular characterization and theoretical study of first generation dendritic homopolymers of butadiene and isoprene with different microstructures

S. Rangou [a], P.E. Theodorakis [a], L.N. Gergidis [a], A. Avgeropoulos [a,*], P. Efthymiopoulos [b], D. Smyrnaios [b], M. Kosmas [b], C. Vlahos [b,**], Th. Giannopoulos [c]

[a] *Department of Materials Science and Engineering, University of Ioannina, Administration Building, University Campus Dourouti, 45110 Ioannina, Greece*
[b] *Department of Chemistry, University Campus Dourouti, University of Ioannina, 45110 Ioannina, Greece*
[c] *Department of Biological Applications and Technology, University Campus Dourouti, University of Ioannina, 45110 Ioannina, Greece*

Received 15 September 2006; received in revised form 16 November 2006; accepted 20 November 2006
Available online 8 December 2006

Abstract

We report the synthesis of first generation dendritic homopolymers consisting of either poly(butadiene) (PB) of 1,4-microstructure or poly(isoprene) enriched in 3,4-microstructure (at least 55% $PI_{3,4}$). The main aspect was the synthesis of polymers exhibiting high molecular and compositional homogeneity. The preparation of these materials was achieved via anionic polymerization techniques in combination with chlorosilane chemistry. The molecular characterization of the final dendritic materials was made via size exclusion chromatography (SEC), membrane osmometry (MO), dilute solution viscometry and ^1H nuclear magnetic resonance (NMR) spectroscopy, leading to the conclusion that they can be considered as model polymers. The conformational properties of the synthesized dendritic polymers were studied by means of analytical theory and Monte Carlo simulations using coarse graining models with the same number of segments. The radii of gyration and the length of the branches of zeroth and first generations were calculated via lattice, off-lattice algorithms, and renormalization group techniques. The theoretical findings were compared with the respective results of star polymers with the same functionality and equivalent branch lengths.

Keywords: Dendritic polymers; Synthesis and characterization; Theoretical study

1. Introduction

Advances in synthetic polymer chemistry and nanotechnology applications of polymers lead to the necessity of designing complex architectures in order to combine the observed properties of more simple structures. Such complex architectured polymeric materials are the dendritic polymers which can be considered as a new type of materials (since they have been evolved approximately two decades ago), exhibiting unique potentials, reasons that made them useful in many applications [1]. A dendritic structure is considered as an architecture including random hyperbranched, dendrigrafts and dendrimers. It is of great importance to differentiate these polymeric materials according to their divergences in properties and behavior. Extreme differences in properties can be attributed to the generation; therefore a large dependence on the complexity of the studied macromolecule is being observed. According to a very recent literature [2] there is a clear distinction in the dendritic polymers depending on the number of generations; therefore when the generation is 0–2 they are called ''cascade molecules'' and when the generation is higher than 2 they are considered as ''dendrimers''. Their synthesis, despite the generation number, is rather difficult and time-consuming. This is a major disadvantage of such materials, leading to a relatively small number of papers referring to the synthesis or

* Corresponding author. Tel.: +30 26510 97316; fax: +30 26510 97034.
** Corresponding author. Tel.: +30 26510 98430; fax: +30 26510 98798.
E-mail addresses: aavger@cc.uoi.gr (A. Avgeropoulos), cvlahos@cc.uoi.gr (C. Vlahos).

0032-3861/$ - see front matter © 2006 Elsevier Ltd. All rights reserved.
doi:10.1016/j.polymer.2006.11.041

characterization of dendrimers. There are reported attempts of producing dendritic materials but most of the times this resulted in complex structured polymers with lack of symmetry and uncontrolled branching degree [3–8]. Other attempts led to materials with wide molecular weight distribution [9,10], which cannot be considered as model polymers.

The successful synthesis of dendritic homopolymers has previously been reported. First Al-Muallem et al. [11–13] have reported the synthesis of dendritic polystyrene of the $(S_4S')_4$ type. They worked on the basis of anionic polymerization and used 4-(chlorodimethylsilyl)styrene or 4-(chloromethyl)styrene as linking agent, under inert gas atmosphere, following a one-step synthetic technology. Based on that work and high vacuum techniques Chalari and Hadjichristidis [14] were able to synthesize first generation dendritic homopolymers consisting of polystyrene or poly(isoprene) (exhibiting ~90% 1,4-microstructure), exhibiting both molecular and compositional homogeneity.

In this paper, we refer experimentally to the synthesis and molecular characterization of first generation dendritic homopolymers of poly(butadiene) (with ~92% 1,4-microstructure) and poly(isoprene) (with increased 3,4-microstructure), with narrow polydispersities. A first generation dendritic homopolymer is exhibited in Scheme 1.

The differences in the microstructure of the reported dendritic polymers are expected to lead to a very different behavior in melts and blends which is one of the issues discussed in this work. It is expected that in dilute solutions these differences will be negligible, and thus coarse graining models can be used to satisfactorily describe their conformational properties.

The conformational behavior of dendritic homopolymers has been studied extensively via Monte Carlo [15–20] and analytical methods [21–23]. The interest of the theoretical studies is mainly concentrated on three of their properties useful for daily applications. First, the dendritic macromolecules can have a high surface and numerous terminal ends. This leads to high density of the end groups leading to enhanced catalytic activity or high reactivity generally, depending on the aimed task. The second useful property comes from the density fluctuations and cavities, which are positive for the use of these materials as carriers of small molecules. This second property is often combined with their third property of the capability of an increased permeability to the interior of a macromolecule. The Monte Carlo studies, however, are mainly limited in the study of dendrimers with very short branches, which are almost hard spheres. In this work, we study the synthesized dendritic polymers of first generation, which consist of flexible macromolecular branches in order to find how the branch length affects their above mentioned properties. We employ off-lattice (pivot algorithm) and lattice simulations (bond fluctuation model) as well as renormalization group theory using our previous experience on studies concerned with macromolecules of complicated architectures [24–27]. The conformational properties of the first generation dendritic polymers are compared with the respective properties of star polymers in order to investigate how this complex architecture influences the sizes of various parts of the dendritic macromolecule. Both analytical and computational models have advantages and disadvantages, but the combination of these methods is expected to give a clear view of their properties.

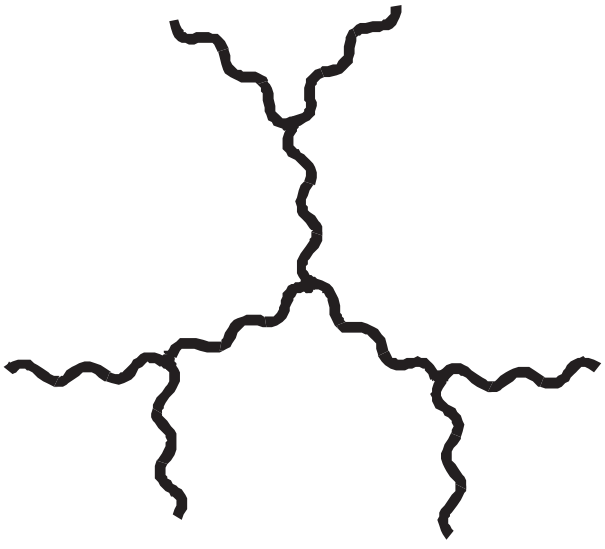

Scheme 1. Schematic presentation of a first generation dendritic homopolymer.

2. Experimental part

2.1. Materials

All samples were prepared via anionic polymerization using high vacuum techniques in evacuated, *n*-BuLi washed and benzene rinsed glass vessels. Analytical information on the high vacuum technique as well as the purification procedures for the monomers (butadiene, isoprene), solvents [benzene, tetrahydrofuran (THF)] and initiator (*sec*-BuLi) to the standards required for anionic polymerization have been described in detail elsewhere [28]. 4-(Chlorodimethylsilyl)styrene was synthesized from *p*-chlorostyrene and dichlorodimethylsilane through a Grignard reaction, under high vacuum techniques. *p*-Chlorostyrene was purified by distillation over CaH_2 and was stored at −20 °C in sealed ampules. The magnesium (Aldrich) used in the Grignard reaction was dried in a vacuum oven at 40 °C for two days in order to completely remove any humidity traces prior to use. The magnesium was activated via 1,2-dibromoethane (Fluka) in THF. The completion of the reaction and the successful synthesis of the required 4-(chlorodimethylsilyl)styrene (CDMSS) was observed via gas chromatography–mass spectroscopy (GC–MS), where no traces of the initial reactants were obtained. Through the GC–MS technique we were able to completely comprehend the yield of the reaction. More details of the whole Grignard synthesis process are given elsewhere [14].

2.2. Polymer synthesis

2.2.1. $[(PB)_2PB]_3$ (1st G-hPB-10K)

The poly(butadiene) living chain was synthesized by polymerizing 10 g of butadiene (0.135 mol) with *sec*-BuLi

(0.1 mmol), in 150 ml of benzene at room temperature for 24 h. The molecular weight of the living chain was approximately 10,000 g/mol. It was divided in two ampules (approximate concentration of the living chain $PB^{(-)}Li^{(+)}$ was 0.05 mmol in each one). The first quantity was added dropwise in the CDMSS solution (0.05 mmol in 10 ml of benzene) leading to the formation of the macromonomer. The addition of the poly(butadiene) living chain was accomplished via titration and controlled by collecting aliquots during the reaction. SEC experiments were performed to verify the progress of the titration reaction. The solution was then added in the second ampule containing the remaining living chain in order to link the two chains creating the macroinitiator. Polymerization of 7 g or 0.9 mol of butadiene is initiated by the macroinitiator and completed within 24 h. After the completion of the polymerization, trichloromethylsilane (0.025 mmol) is added in the flask and the linking reaction is left to be completed for 25 days. Again, SEC instrumentation is used to control the reactions leading to the precursors, the intermediate and the final products.

2.2.2. $[(PI)_2PI]_3$ (1st G-hPI-10K)

The difference in the synthesis of the first generation homopoly(isoprene) is the fact that during the synthesis of the initial $PI^{(-)}Li^{(+)}$ chain a small amount of THF is used in order to alter the microstructure of the segments. The polymer synthesis is accomplished by following the steps described above for the $[(PB)_2PB]_3$ case.

2.3. Molecular characterization

The GC–MS instrument was equipped with a split/splitless injector and an MDN-5 column (Supelco) was used for separation (30 m × 0.25 mm i.d., 0.25-μm film thickness). The temperature program for the GC-17A interfaced with a QP5000 MS was as follows: the GC oven temperature started at 100 °C, after 3 min the column was heated at 10 °C/min to 280 °C. The total run time was 21 min. The mass spectrometer started its run 3 min after the injection where by the mass ranging from 50 to 500 was recorded. The control of the GC–MS system and the evaluation of the chromatograms received were carried out by means of CLASS-5000 Version 1.24 Chromatography Software (Shimadzu Chem. Lab. Analysis System and Software).

The molecular characterization was carried out by size exclusion chromatography (SEC), membrane osmometry (MO) and vapor pressure osmometry (VPO). The number-average molecular weights ($\overline{M}_n$) (higher than 15,000 g/mol) of the precursors and the final products were measured with a Gonotec Membrane Osmometer (MO) Osmomat 090 at 35 °C. Toluene, distilled over CaH_2, was the measuring solvent. The $\overline{M}_n$ values for the MO measurements were determined from the $\sqrt{\pi/c}$ versus c plots (π is the osmotic pressure and c is the concentration). Square root plots were used in order to minimize the curvature due to the third virial coefficient. More details are given elsewhere [29]. In all cases the correlation coefficient was better than 0.99. Number-average molecular weights ($\overline{M}_n$) (lower than 15,000 g/mol) of the precursors were measured with a Gonotec Membrane Osmometer (MO) Osmomat 070 at 50 °C in toluene, which was calibrated with a benzyl solution to determine the consistency of the instrument.

SEC was calibrated with eight PS standards ($\overline{M}_w$: 4.3–3000 kg/mol) and always prior to calculating the polydispersity indices of the unknown materials. A series of standard PS solutions were tested in order to examine the accuracy of the instrumentation.

^{1}H NMR determination of the composition and the microstructure of the materials was carried out in $CDCl_3$ at 30 °C using a Bruker AVANCE II spectrometer. Data were processed using UXNMR (Bruker) software. The typical microstructure which is characteristic of anionic polymerization of butadiene in benzene (92 wt% − 1,4 and 8 wt% − 1,2) was observed for the PB dendritic homopolymers. For the poly(isoprene) corresponding materials a microstructure was observed different from that of the usual anionic polymerization of isoprene in benzene. Since a small quantity of polar solvent was used (THF, <1 ml), the microstructure of PI was calculated to be approximately ~55 wt% − 3,4, 15 wt% − 1,2 and 30 wt% − 1,4. The lower 1,4-content is due to the delocalization of the negative charge among the three final carbons of the living chain (loose ion pairs). Additionally ^{1}H NMR was used to confirm the synthesis of 4-(chlorodimethylsilyl)styrene after the conversion of the Si–Cl group to Si–OH and exhibited the following results: 7.40–7.60 (C_6H_4), 6.70–6.80 (CH_2=C*H*), 5.40–5.90 (C*H*$_2$=CH), ~2.20 (–Si–OH) and 0.20–0.35 ppm ($(CH_3)_2$–Si–), leading to the expected ratios of the protons after integration.

The viscometry measurements were accomplished by using a type 0c Ubbelohde suspended level dilution viscometer (suitable only for toluene) at a thermo stated water bath of 35 °C. Toluene is a common good solvent for PB and PI chains. The solvent was refluxed over CaH_2 for 24 h and was fractionally distilled prior to use.

3. Experimental results and discussion

The Grignard reaction necessary to synthesize the linking reagent for preparing the first intermediate product is shown in Scheme 2. The success of the reaction has appeared to be rather crucial for the completion of the polymerization reactions and the preparation of the final dendritic homopolymers. GC–MS and ^{1}H NMR studies were made in order to completely control the final product of the Grignard reaction, after distillation, leading to large purity (higher than 99%).

First, a living polymer chain ($PB^{(-)}Li^{(+)}$ or $PI^{(-)}Li^{(+)}$) was reacted selectively with the chlorosilane group of 4-(chlorodimethylsilyl)styrene and the equivalent macromonomer was produced. The synthetic strategy of the macromonomers is the addition of stoichiometric amount of the living chain in the solution of the coupling agent. The macromolecular segment is terminated by the reaction of the living end with the chlorosilyl group and LiCl is being produced. This is followed by the slow addition of the previously described macromonomer into the solution of the second living chain ($PB^{(-)}Li^{(+)}$ or

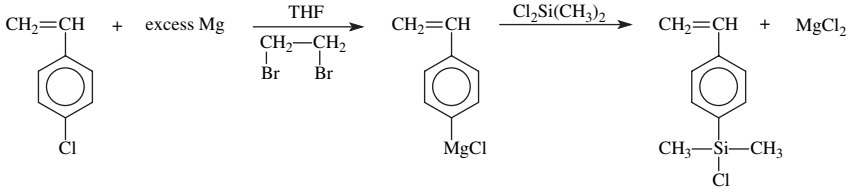

Scheme 2. Synthesis of the Grignard reagent.

$PI^{(-)}Li^{(+)}$), whose functionality leads to the addition through the vinyl bond of the initial macromonomer. The substitution of the chlorosilyl group is easier than the addition of the vinyl bond and this is the reason why the second addition is much slower [30]. The necessary amount of monomer is then polymerized leading to the monofunctional zeroth generation homopolymer, as observed in Scheme 3.

The addition of living chains to CDMSS leading to the macromonomer was achieved through end capping with 2–3 monomeric units of styrene. With this approach the living ends were altered to $PS^{(-)}Li^{(+)}$ leading to better control of the linking reaction.

It should be pointed that in the case of PI all the polymeric chains where of the same microstructure (increased 3,4-), but in the case of the PB the first two chains where exhibiting the usual microstructure of 92% − 1,4 and 8% − 1,2. When the necessary amount of the butadiene was added to synthesize the monofunctional zeroth generation homopolymer, due to the existence of THF, the microstructure was altered and was increased in 1,2-content. An experiment for creating a simple PB homopolymer with the presence of small amount of THF was made in order to study and calculate the microstructure. We found from ^{1}H NMR that the microstructure was approximately 60% − 1,2 and 40% − 1,4. Therefore, the dendritic PB polymers synthesized in this work may be considered as copolymers instead of homopolymers. This is due to the fact that alternation of the microstructure may differentiate the Flory–Huggins interaction parameter, χ, between the two different chains, as previously reported in the literature by Cohen and Willfong [31]. They have calculated χ for different diene pairs, obtaining room temperature values of 0.081 and 0.048 for 1,4-PI/1,4-PB and 1,4-PI/1,2-PB, respectively. A set of experimental results have also been reported, in the aforementioned literature, for the particular binary system 1,2-PB/1,4-PB, where χ is predominantly different from zero.

Finally the coupling of the monofunctional zeroth generation homopolymer with (trichloromethyl)silane (CH_3SiCl_3) is achieved. In this way the equivalent first generation homopolymer is being synthesized, the synthesis and structure of which are shown in Scheme 4. The molecular characterization results form SEC, MO (in some cases of the initial homopolymers VPO was used) and viscometry are shown in Table 1. The values given for the $\overline{M}_w$ provided by the combination of SEC and osmometry and those exhibited from the viscometry measurements are approximately equal. It should be noted that in most cases of anionically synthesized polymers the intrinsic molecular weight calculated by viscometry is approximately equal to the $\overline{M}_w$. The low polydispersity indices exhibited by SEC experiments and the value $\overline{M}_w/\overline{M}_n$ provided from viscometry ($\overline{M}_w$) and osmometry ($\overline{M}_n$) are also similar, leading finally to the conclusion that the homopolymers, intermediate

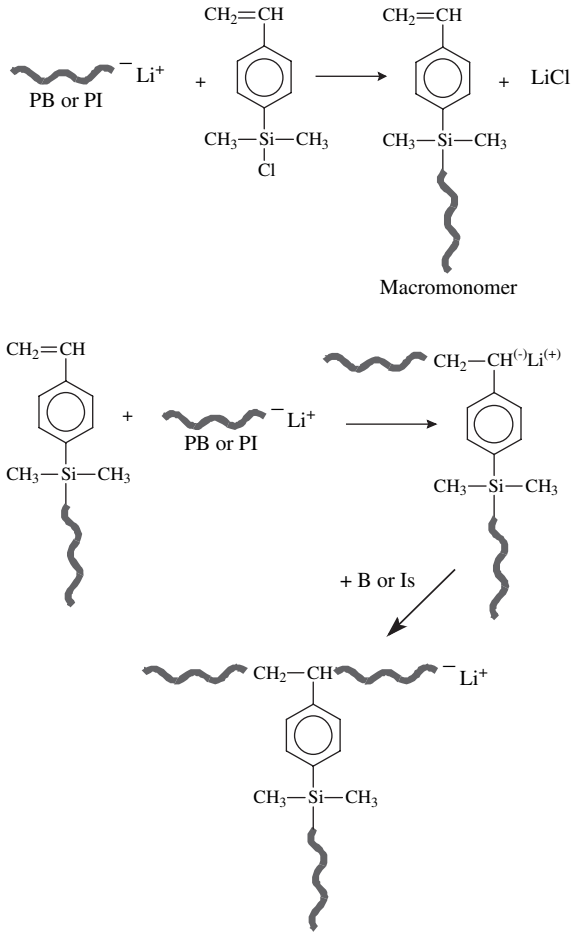

Scheme 3. Synthesis of the macromonomer and the functional zeroth generation homopolymer.

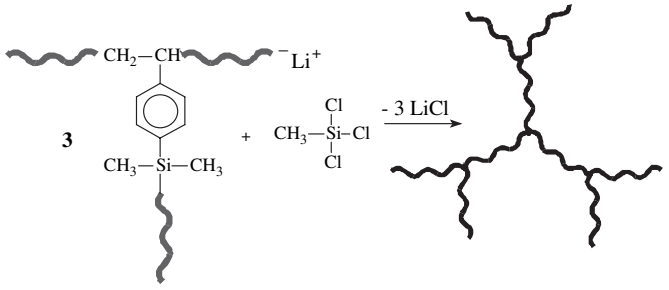

Scheme 4. Synthesis of the first generation homopolymer.

Table 1
Molecular characteristics of the intermediate (initial linear polymer, zeroth generation) and final (first generation) polymers

Sample	Total $\overline{M}_w \times 10^{-3}$ [a]	Total $\overline{M}_n \times 10^{-3}$ [b]	$\overline{M}_w/\overline{M}_n$ [d]	Functionality[e]	Total $\overline{M}_w \times 10^{-3}$ [f]	$<S^2>$ (nm)
PB-10K	10.2	9.8[c]	1.04	–	9.9	17.3
PB-20K	18.6	17.7	1.05	–	17.8	22.1
PI-10K	9.8	9.5[c]	1.03	–	9.4	19.1
PI-20K	21.4	20.4	1.05	–	22.0	25.2
0th G-hPB-10K	30.6	28.9	1.06	–	–	–
0th G-hPB-20K	55.6	52.0	1.07	–	–	–
0th G-hPI-10K	29.4	28.0	1.05	–	–	–
0th G-hPI-20K	64.2	59.4	1.08	–	–	–
1st G-hPB-10K	88.6	82.0	1.08	2.84	86.8	51.2
1st G-hPB-20K	152.7	141.4	1.08	2.72	150.1	60.6
1st G-hPI-10K	85.5	78.4	1.09	2.80	84.7	55.4
1st G-hPI-20K	175.8	162.8	1.08	2.74	177.0	68.1
3-arm star $(PI)_3$	59.8	56.4	1.06	2.90	57.2	41.0

hPB and hPI stands for homopolymer PB and homopolymer PI, respectively.
[a] Calculated from the results obtained from osmometry and SEC.
[b] MO in toluene at 35 °C.
[c] VPO in toluene at 50 °C.
[d] SEC in THF at 30 °C with PS standards.
[e] Using the equation: ($\overline{M}_n$ first G-hpolymer)/($\overline{M}_n$ zeroth G-hpolymer), where hpolymer stands for homopolymer.
[f] Using the equation $\langle \overline{S}^2 \rangle^{3/2} = [\eta]\overline{M}_w/\Phi$, where $[\eta]$ is the intrinsic viscosity, $\overline{M}_w$ is the average molecular weight per weight of the homopolymer and Φ is Flory's constant and equals to 2.5×10^{21} when $[\eta]$ is given in dL/g units.

products and the final dendritic polymers synthesized in this work exhibit molecular and compositional homogeneity. Additionally, from the viscometry technique the calculation of the radius of gyration is carried out in order to compare the experimental results with the theoretical predicted values. More specifically, experimental values of the intrinsic viscosity, $[\eta]$, of the initial homopolymers and the final dendritic homopolymers were provided in a common good solvent (toluene, 35 °C). The values were obtained by extrapolation to zero concentration of η_{sp}/C versus C plots and $\ln(\eta_{rel})/C$ versus C plots (C: concentration). Despite the fact that intrinsic viscosities are commonly used we measured the radius of gyration $\langle S^2 \rangle$ (given in nm) to verify the calculated values with those predicted theoretically. The same experiment was carried out for the three-miktoarm star homopolymer of the $(PI)_3$ type, where each arm was ~20,000 g/mol in molecular weight.

The functionalities deriving from the molecular characterization are provided in Table 1, and indicate a value varying from 2.74 to 2.84. Thus, the number of dendrons linked to create the final dendritic homopolymers is three. It should be noted that the functionality for the 3-miktoarm star is 2.9, a higher value due to the simplicity of the architecture when compared to the dendritic structure.

The achievement of synthesizing the final dendritic samples relied on the use of the end capping technique, as mentioned above. When the living chain ($PI_{3,4}^{(-)}Li^{(+)}$ or $PB^{(-)}Li^{(+)}$) is synthesized a small number of styrenic monomeric units (2–3) are inserted in order to alter the reactivity of the living ends. Their restricted movement leads to easier control of the addition to the 4-(chlorodimethylsilyl)styrene solution in order to substitute its para-positioned chlorine atom. Due to the fact that the dienes are less sterically hindered, the adaptation of the styrene at the end of the second living chain is repeated before its addition to the linking agent, in order to better control the addition to the vinyl bond. This approach is different from that reported already by Chalari and Hadjichristidis [14]. Better control of the synthesis and less termination phenomena were observed in our case as shown in Fig. 1, where the SEC chromatograms of initial, intermediate and final products are exhibited.

It is clearly understood from the chromatographs at Fig. 1 that in order to obtain the final dendritic homopolymers, as pure as possible, fractionation techniques were adopted using a solvent (toluene)/non-solvent (methanol) system. As indicated in Fig. 1 the fractionation worked successfully since rather easily the final first generation homopolymers were separated from all other products.

The main difference between the dendritic poly(isoprene) homopolymers referred previously [14] and those we composed is the totally different microstructure of the poly(isoprene) that is synthesized via anionic polymerization

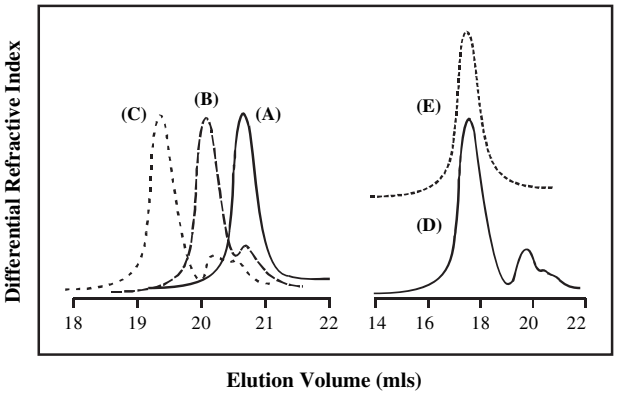

Fig. 1. SEC chromatographs of (A) PB homopolymer with approximate number-average molecular weight ($\overline{M}_n$) 10,000 g/mol, (B) $(PB)_2$-macroinitiator, (C) living $(PB)_3$ zeroth generation homopolymer prior to linking with CH_3SiCl_3, (D) unfractionated first generation dendritic homopolymer of the $[(PB)_2PB]_3$ type and (E) fractionated first generation dendritic homopolymer of the $[(PB)_2PB]_3$ type.

techniques in non-polar environment. The molecular weights of the samples reported in this paper were approximately 10,000 g/mol and 20,000 g/mol for each branch for both $[(PB)_2PB]_3$ and $[(PI)_2PI]_3$ types. In our case, especially for the $[(PI)_2PI]_3$ type, the addition of just a small amount of polar solvent (THF) has dramatic effect on the observed microstructure of the synthesized PI chains. Specifically, in a non-polar synthesis procedure the resultant microstructure of a PI is 90 wt% 1,4- (70% *cis* and 20% *trans*) and 10 wt% 3,4-microstructure, whereas in polar environment the 3,4-microstructure of PI is highly increased ($\sim$50–60%) and the 1,2-microstructure is increased as well (15–25%).

4. Theoretical part

4.1. Monte Carlo simulations

4.1.1. Off-lattice model

We consider a trifunctional dendritic homopolymer of first generation (Fig. 2). Each of the nine arms contains N beads. The central unit of the zeroth generation is the common origin of coordinates and is assigned as unit $9N+1$. Non-neighbouring units interact through Lennard-Jones potentials:

$$U(R_{ij})/k_BT = 4(\varepsilon/k_BT)\left[(\sigma/R_{ij})^{12} - (\sigma/R_{ij})^{6}\right] \quad (1)$$

where ε is the interaction energy between units, R_{ij} is the separation distance between units i and j and σ a steric parameter considered the same for all units. To reproduce the macroscopic state, of good solvent, we adopt previously reported set of Lennard-Jones parameters ($\varepsilon/k_BT = 0.1$, $\sigma = 0.8$) [32]. This set of values reproduces the universal critical exponent $\nu = 3/5$ of the radius of gyration ($\langle S^2\rangle \sim N^{2\nu}$). The value $\varepsilon/k_BT = 0$ corresponds to the ideal (Gaussian) θ chain without interactions between units. The properties of interest are the mean end-to-end square distances of the arms of the zeroth and first generations, as well as the angles X, Y, Z illustrated in Fig. 2. We also estimate the radius of gyration of the whole dendritic macromolecule and the radii of gyration of each generation. The high efficient pivot algorithm is used for the Monte Carlo sampling. It starts by building an initial configuration of moderate energy and then a bead is selected at random. If the selected bead belongs to the first generation, the rest of the beads on the selected arm up to the closest end are rotated according to three randomly chosen Euler angles. Otherwise, if the selected bead belongs to zeroth generation, the rest of the beads on the selected arm and the units on the following two arms of the first generation are rotated. The metropolis energy criterion is used to test the acceptance or rejection of the new trial configuration. Ten independent runs are performed. Each run attempts 200.000–10^6 configurations after appropriate thermalization. The properties are firstly averaged over all conformations in each run, and then the mean values and the standard deviations are determined from the 10 independent runs.

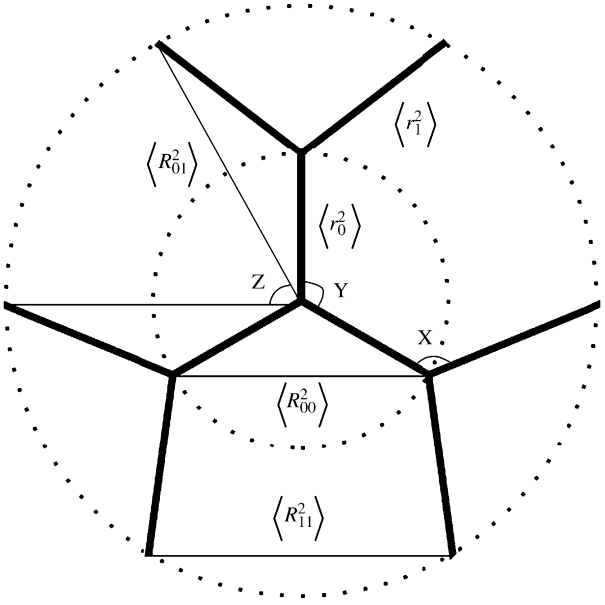

Fig. 2. The mean end-to-end square distances for some specific combinations of branches and the corresponding angles between them.

4.1.2. Bond fluctuation model (BFM)

In the bond fluctuation model [33] we place a single trifunctional first generation dendritic homopolymer composed of $9N+1$ units in a simple cubic lattice of length L with periodic boundary conditions. The distance between adjusted sites b, is taken as the unit of length. Each unit blocks the other 26 lattice sites contained in the elementary cube and is centered at the bead location. In this way, the model complies with the restriction imposed for self-avoiding walk (SAW) polymers. Bonds linking the beads can have lengths ranging between 2 and $\sqrt{10}$, but bond vectors of the type (±2, ±2, 0) are excluded in order to avoid bond crossing during the simulation. Equilibration is performed from the initial configurations through elementary bead jump, with displacement vectors (±1, 0, 0), (0, ±1, 0) and (0, 0, ±1). Once the move has been made, the lengths of the new bonds are checked for compliance with the BFM lengths. To facilitate further the mobility of dendritic chain, a larger area of blocked lattice sites is established around the central unit of the zeroth generation and around the last unit of each arm of the zeroth generation, which can also be considered as central units of the first generation arms. The distance between the central units and its first neighbours is permitted to increase up to 5, instead of the value $\sqrt{10}$ established for the other units. The new configuration is accepted if the SAW condition is fulfilled. Typically 5×10^6 Monte Carlo steps are attempted for equilibration followed by the same number of steps for the calculation of properties. As in the case of off-lattice simulations, the properties, mean values and the standard deviations, are determined from 10 independent runs.

4.1.3. Renormalization group theory (RG)

Following our previous work [26] we write the probability distribution function of the first generation dendritic polymer with functionality f and branch length N as:

$$P[R(s)] = P_0[R(s)]\exp\left\{ -u \iint \mathrm{d}s_a \mathrm{d}s_{a'} \delta[R(s_a) - R(s_{a'})] \right\}, \tag{2}$$

where $R(s)$ is the position vector of each point at the contour length s of the chain considered as a continuous line and $P_0[R(s)]$ is the ideal connectivity term of the Gaussian type. δ is the d-dimensional Dirac delta function which brings in contact all pairs of units coming from the same or different branches and u is the excluded volume interaction parameter. Our description and analysis is based on the mean end-to-end square distances of all possible branches, as well as on specific combination of them $\langle r_0^2\rangle$, $\langle r_1^2\rangle$, $\langle R_{00}^2\rangle$, $\langle R_{01}^2\rangle$, $\langle R_{11}^2\rangle$ shown in Fig. 2. By means of the squares of these distances considered to form triangles, three effective angles are defined as:

$$X = \cos^{-1}\left[\left(\langle r_0^2\rangle + \langle r_1^2\rangle - \langle R_{01}^2\rangle \right) / 2\sqrt{\langle r_0^2\rangle \langle r_1^2\rangle} \right] \tag{3}$$

$$Y = \cos^{-1}\left[\left(2\langle r_0^2\rangle - \langle R_{00}^2\rangle \right) / 2\langle r_0^2\rangle \right] \tag{4}$$

$$Z = \cos^{-1}\left[\left(2\langle R_{01}^2\rangle - \langle R_{11}^2\rangle \right) / 2\langle R_{01}^2\rangle \right]. \tag{5}$$

They can be used in order to specify to a first approximation, the relative positions of the end of branches, the emptiness in the interior of the dendritic polymer and the capability to carry guest molecules.

In the canonical ensemble the mean end-to-end square distances are obtained as:

$$\langle R^2\rangle = \left\{ \int D[r(s)] R^2 P[R(s)] \right\} \Big/ \left\{ \int D[r(s)] P[R(s)] \right\} \tag{6}$$

where $D[R(s)]$ is the measure of the path integrals, which expresses the integrations over all points of the chain in the continuous line limit. Expanding the exponential terms both in numerator and denominator up to the first order of the excluded volume interaction parameter u, we take expressions of the form:

$$\langle R^2\rangle = \langle R^2\rangle_0 \left\{ 1 + u \iint F(i,j)\mathrm{d}i\mathrm{d}j \right\} \tag{7}$$

where $\langle R^2\rangle_0$ is the ideal chain result. When the unit length is equal to one, then $\langle r_0^2\rangle_0$, $\langle r_1^2\rangle_0$, $\langle R_{00}^2\rangle_0$, $\langle R_{01}^2\rangle_0$ and $\langle R_{11}^2\rangle_0$ are equal to N, N, $2N$, $2N$ and $4N$, respectively. The F functions include the contribution of the dendritic architecture with the indices i, j running all over the contour length of the macromolecule.

5. Theoretical results and discussion

The diagrammatic expressions of the above properties for the space dimensionality $d = 4$, which give results to order $\varepsilon = 4 - d$ [24], are given in the Appendix A. Performing the necessary i, j integrations (Appendix B), we arrive to the analytical expressions presented in Appendix C. It can be observed that the mean end-to-end square distance of a branch of the zeroth generation $\langle r_0^2\rangle$ increases linearly by enhancing the solvent quality since the intensity of excluded volume interactions u increases as well. It also increases by increasing the functionality of the dendritic polymer, with f being to the power of 3, due to the presence of more interacting units coming from both generations in the vicinity of the branch. The respective property of a star polymer chain with the same functionality and the same branch length $\langle R^2\rangle_{\mathrm{star}}$ is also given in the Appendix C for comparison purposes. In the analytical expression of $\langle r_0^2\rangle$ of the dendritic polymer $\langle r_0^2\rangle = N\{1 + u[2\ln N + F_{\mathrm{d0}}(f)]\}$, we find that the constant term $F_{\mathrm{d0}}(f)$ ($F_{\mathrm{d0}}(3) = 4.571$, $F_{\mathrm{d0}}(6) = 30.34$) is higher than the respective term $F_{\mathrm{s}}(f)$ ($F_{\mathrm{s}}(3) = -0.227$, $F_{\mathrm{s}}(6) = 2.43$) of $\langle R^2\rangle_{\mathrm{star}}$ of a star polymer branch. This indicates that the branches of the zeroth generation are more expanded compared to those of an equivalent star polymer, due to the interactions with the back folding units of the first generation. The mean end-to-end distance $\langle r_1^2\rangle$ of the arms of the first generation shows the same qualitative behavior with the $\langle r_0^2\rangle$ when the excluded volume interactions, the functionality and the molecular weight change. From the analytical expressions of $\langle r_0^2\rangle$ and $\langle r_1^2\rangle$, we find that the branches of the two different generations are not equivalent. The interior ones are more expanded since their constant terms are greater than the respective terms of the outer branches ($F_{\mathrm{d1}}(3) = -0.006$, $F_{\mathrm{d1}}(6) = 3.30$). In the limit of long arms the logarithmic term dominates over the constant term $\ln N >> F(f)$ and the critical exponent of the mean end-to-end square distances is obtained by means of the fixed point value $u^* = \varepsilon/16(\langle r^2\rangle = N\{1 + u2\ln N\} \sim N^{1+2u^*})$ for good solvent conditions. This exponent is identical to the one we found in the cases of linear and star polymers. However, the novelty in the case of dendritic polymers is that the end-to-end square distances of branches of the outer generations reaches the exponential regime for shorter arms contrary to the interior generations. This may affect the critical exponents of conformational properties including all generations such as the radius of gyration of the whole molecule and especially the exponents obtained by means of Monte Carlo simulations, where the arm lengths are very short. The rest of the properties in the Appendix C are the diameters of the two different generations $\langle R_{00}^2\rangle$ and $\langle R_{11}^2\rangle$ and the respective star polymers $\langle D_{\mathrm{star}}^2\rangle$, which are necessary for the calculation of the three angles of interest X, Y and Z presented in Fig. 2.

Special characteristic graphs of the angles are given for the understanding of their general behavior (Figs. 3 and 4). When the angle X is large the end beads are mainly in the outside region of the polymer and they are very active, while for small values of X they turn inside the polymer matrix and their activity is hindered. The angle Y between the position vectors of the two ends of the arms of the zeroth generation indicates the empty spaces that the interior region can have. For larger angles Y, larger emptiness in the interior of the dendritic polymer is expected. Hence, the capability to carry guest molecules is higher. The passage of the cargos to the interior of the dendritic molecule is described by means of the third angle Z formed by the vectors R_{01}. In Fig. 3 the effect of the

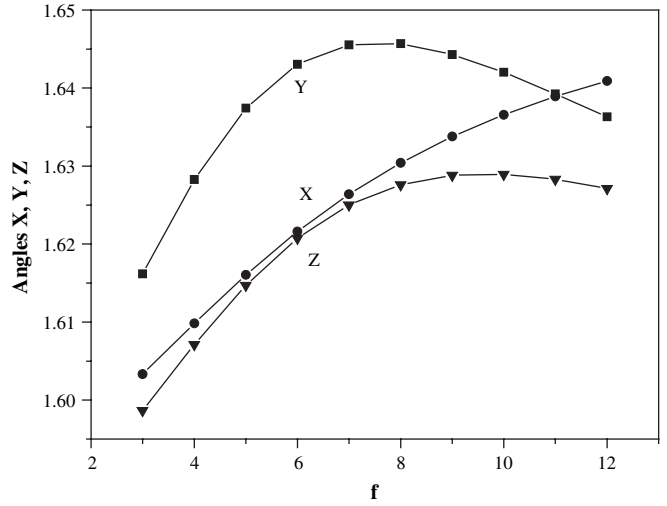

Fig. 3. The dependence of the angles X, Y, Z on the functionality f of the dendritic chain in good solvent conditions obtained by RG theory ($N = 100$, $u^* = 1/16$).

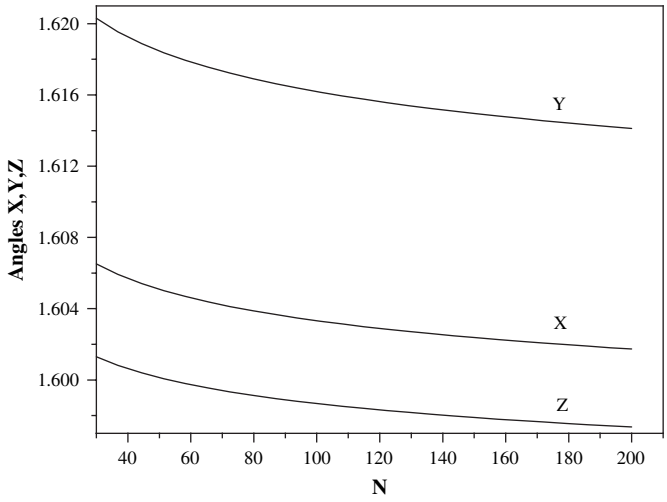

Fig. 4. The dependence of the angles X, Y, Z on the dendritic branch molecular weight N in good solvent conditions obtained by RG theory ($f = 3$, $u^* = 1/16$).

functionality f is examined for dendritic polymers with arm length $N = 100$.

By increasing f, Y is increasing up to $f = 8$ where the maximum free space in the interior of the dendritic polymer is obtained. Further increase of functionality f leads to lower values of Y. The same trends are also obtained for the angle Z. The maximum size of the appropriate guest molecules to enter is obtained for $f = 10$, whereas further increase of f leads to smaller values of Z. The activity of dendritic ends (angle X) is increased by increasing f since the arms become stiffer, due to the excluded volume interactions. The maximum value of X is obtained for $f = 30$ (not shown in the graph). Further increase of f leads to a dense core, where the excluded volume interactions are reduced, leading to smaller values of X. In the limit of large f the excluded volume interactions are canceled and X approaches the value of the Gaussian chain $\pi/2$ (1.57 rad). The effect of the arm molecular weight on the three angles is illustrated in Fig. 4.

For repulsions between units ($u > 0$) the main tendency of all angles is to decrease on increasing branch length N. The explanation of this behavior lies on the existence of a common origin of the arms of the first generation which force them to be close in space. Because of the proximity of the branches the monomeric repulsions expand them towards the outer space making the interior branches more extended. The extension of the arms of the zeroth generation permits their ends to come closer in space thus reducing both the Y and Z angles. The expansion of the arms of zeroth generation reduces the density in the interior region and the angle X is also reduced on increasing N, because the ends of the first generation can be easily turned into the less dense region of the zeroth generation. In the limit of infinite branch length the logarithmic terms dominate over the constant terms $F(f)$ and the nominator of the Eqs. (3)–(5) describing the angles X, Y and Z diminishes and finally the ideal values of the Gaussian chains $\pi/2$ (1.57 rad) for all angles is obtained.

To check the validity of the analytical results we perform extensive Monte Carlo simulation study of dendritic polymers in good solvent conditions. We use the two different algorithms, pivot and BFM, which have been previously described. The molecular weights of the arms of the simulated dendritic polymers correspond to the ones we have synthesized in the current paper. Using the C_∞ values 5.53 and 4.80 for the butadiene and isoprene polymers respectively (with particular microstructure [34]), we found that their arm lengths are equal to $N = 30$, 63 and 120 segments. The properties of interest are the same as we have estimated in our analytical study. Moreover, we calculate the radii of gyration of the zeroth generation and the whole dendritic polymer. In addition, we computed the radii of gyration of star polymers with functionality $f = 3$ and branch lengths equal to 30, 60, 63, 120 and 126. From the properties above, dimensionless ratios, which are independent of the Kuhn length, are obtained and they are presented in Tables 2 and 3. In the same tables, we also include the RG results regarding the dimensionless ratios for the good solvent conditions ($u = u^* = 1/16$). According to the ratio $\langle r_0^2\rangle/\langle r_1^2\rangle$ (Table 2), the RG results clearly show that the interior branches are more expanded than the outer branches due to the high density of units close to the dendritic molecule origin.

These analytical results lie between the ones obtained by both Monte Carlo simulation algorithms. The BFM algorithm shows even a higher expansion of the interior branches while the pivot algorithm finds the two different branches to be of almost equal length. The same behavior between the analytical theory and the simulations is obtained for the ratio between the interior branches of dendritic polymer and the branches of star polymer with the same functionality and arm lengths. The interior arms are more expanded, due to the excluded volume interactions arising from the presence of the exterior branches. By increasing the arm length this expansion becomes smaller (about 2%) according to the RG data. However, in Monte Carlo results the standard deviation is about 1, 2 or 5% (depending on the algorithm), which is doubled when we calculate the dimensionless ratios. Hence, this decreasing behavior with increasing molecular weight cannot be verified. For

Table 2
Dimensionless ratios for the macroscopic state of good solvent

Branch length N	RG	MC_pivot	MC_BFM
$\langle r_0^2\rangle/\langle r_1^2\rangle$			
30	1.168	0.987 ± 0.094	1.239 ± 0.014
63	1.158	0.975 ± 0.075	1.263 ± 0.038
120	1.150	1.006 ± 0.047	
$\langle r_0^2\rangle/\langle R_{01}^2\rangle$			
30	0.520	0.452 ± 0.038	0.502 ± 0.008
63	0.519	0.452 ± 0.039	0.501 ± 0.022
120	0.518	0.461 ± 0.026	
$\langle r_0^2\rangle/\langle R_{\mathrm{star}(N)}^2\rangle$			
30	1.179	1.19 ± 0.12	1.274 ± 0.018
63	1.168	1.23 ± 0.13	1.241 ± 0.049
120	1.160	1.203 ± 0.082	
$\langle R_{01}^2\rangle/\langle R_{\mathrm{star}(2N)}^2\rangle$			
30	1.068	1.173 ± 0.087	1.079 ± 0.017
63	1.064	1.185 ± 0.076	1.075 ± 0.040
120	1.061	1.170 ± 0.075	
$\langle S_0^2\rangle/\langle S_{\mathrm{star}(N)}^2\rangle$			
30		1.10 ± 0.12	1.100 ± 0.012
63		1.13 ± 0.13	1.126 ± 0.043
120		1.110 ± 0.055	
$\langle S_{\mathrm{dendr}}^2\rangle/\langle S_{\mathrm{star}(2N)}^2\rangle$			
30		1.362 ± 0.099	1.288 ± 0.027
63		1.375 ± 0.090	1.290 ± 0.054
120		1.365 ± 0.075	

Table 3
The values of the X, Y, Z angles for dendritic and star polymers with $f = 3$ for the macroscopic state of good solvents

Branch length N	RG	MC_pivot	MC_BFM
Angle X			
30	1.607	1.747 ± 0.020	1.696 ± 0.006
63	1.604	1.743 ± 0.017	1.665 ± 0.008
120	1.603	1.735 ± 0.027	
Angle Y			
30	1.620	2.436 ± 0.015	1.762 ± 0.007
63	1.618	2.447 ± 0.015	1.778 ± 0.015
120	1.616	2.435 ± 0.013	
Angle Z			
30	1.601	1.606 ± 0.014	1.716 ± 0.008
63	1.600	1.606 ± 0.006	1.719 ± 0.009
120	1.598	1.609 ± 0.015	
Angle Y (star)			
30	1.593	1.664 ± 0.016	1.700 ± 0.007
63	1.592	1.647 ± 0.024	1.682 ± 0.011
120	1.591	1.646 ± 0.027	

the ratios of the radii of gyration we do not have analytical results. Nevertheless, the Monte Carlo data shows that the radius of gyration of the inner generation of the dendritic polymer is greater than the radius of gyration of star polymer with the same molecular weight. The expansion of the radius of gyration ($\langle S_0^2\rangle/\langle S_{\mathrm{star}(N)}^2\rangle$) is smaller than the expansion of the branches ($\langle r_0^2\rangle/\langle R_{\mathrm{star}(N)}^2\rangle$) according to both algorithms. For the ratio of the radii of gyration of the whole dendritic polymer with branch length N to the star polymer with branch length $2N$ $\langle S_{\mathrm{dendr}}^2\rangle/\langle S_{\mathrm{star}(2N)}^2\rangle$, we have obtained experimental results. This ratio gives an estimation of the size of dendritic polymer in comparison with the star polymer. Intrinsic viscosity measurements of poly(isoprene) dendritic polymer with arm molecular weight of 10K (30 segments) and poly(isoprene) trifunctional star with arm molecular weight of 20K lead to a ratio of hydrodynamic radii of gyration equal to 1.351 (55.4/41.0, as given in Table 1). The experimental value lies between the ones obtained by means of the pivot and BFM algorithms (1.362 and 1.288, respectively) presented in Table 2. This may indicate that the RG values which are also bounded by the Monte Carlo ones can be considered to be closer to the real ones. The different performance of the two Monte Carlo algorithms is more obvious in the estimation of the angles X, Y, and Z presented in Table 3.

For the angle Y (between the inner arms of dendritic polymer) the pivot algorithm values differ significantly from the ones obtained by BFM and the RG theory. Such a difference, however, is not observed for the respective angle Y of star polymers, where both Monte Carlo and RG results are in very good agreement. Although the pivot algorithm gives excellent results in the study of star macromolecules, it has some problems with the movement acceptance in the case of the dendritic polymers, especially when the interior units are chosen. The rotation of the whole sub-tree needs a lot of free space resulting in large values of Y, and thus it influences the other macroscopic properties. On the other hand, the BFM algorithm has some mobility problems with the central units of the exterior arms. The position of these units (which actually are the last units of the interior arms) influences mainly the end-to-end square distances of the interior arms and in some degree, the other conformational averages. The first order analytical results have also been criticized for overestimation of the excluded volume interactions, especially close to the star centers with $f > 6$, where the concentration of units is high enough. However, for our trifunctional dendritic polymers (nine arms) this overestimation should be very small, increasing only for dendritic macromolecules with high functionalities.

6. Conclusions

The synthesis of first generation dendritic homopolymers consisting of either poly(butadiene) (PB) of 1,4-microstructure or poly(isoprene) with high in 3,4-microstructure (at least 55% $PI_{3,4}$), which was achieved via anionic polymerization techniques in combination with chlorosilane chemistry was accomplished. The molecular characterization of the final dendritic materials leads to the conclusion that they can be considered as model polymers, since they exhibited high molecular and compositional homogeneity. The conformational properties of the dendritic polymers were studied by means of analytical theory and Monte Carlo simulations using coarse graining models. We found that the inner arms are more expanded than the outer branches by about 15% for the synthesized dendritic polymers. The activity of the dendritic ends is increased by increasing the functionality reaching a maximum value which depends on the branch length. The empty space in the interior of the dendritic macromolecule and the maximum size of guest molecules is also a non-monotonic function of the

dendritic functionality. By increasing the branch length N all the above quantities are decreasing. At the limit of infinite N, the influence of the dendritic architecture disappears and the dendritic polymer reaches the exponential regime behaving as a linear chain.

Acknowledgements

This research was co-funded by the European Union in the framework of the program "Pythagoras I" of the "Operational Program for Education and Initial Vocational Training" of the 3rd Community Support Framework of the Hellenic Ministry of Education, funded by 25% from national sources and by 75% from the European Social Fund (ESF).

L.N.G. would like to thank Prof. A. Charalambopoulos for helpful discussions. The Laboratory of Mathematical Modeling and Scientific Computations of the Department of Materials Science and Engineering is also acknowledged for generously providing part of the computer resources used in this work.

Appendix A

The diagrammatic expressions of the end-to-end square distances of all possible branches $\langle r_0^2 \rangle$, $\langle r_1^2 \rangle$ and $\langle R_{01}^2 \rangle$ and the respective expressions for the diameters of the zeroth generation $\langle R_{00}^2 \rangle$ and the whole dendritic chain $\langle R_{11}^2 \rangle$.

$$\langle r_0^2 \rangle = N + 2u \Big[\; + 2(f-1) \; + (f-1)^2 \; + \; + (f-1)^2 \; + (f-1)^3 \; \Big]$$

$$\langle r_1^2 \rangle = N + 2u \Big[\; + (f-1) \; + (f-1) \; + \; + (f-1)^2 \; \Big]$$

$$\langle R_{01}^2 \rangle = 2N + 2u \Big[\; 2 \; + \; + (3f-5) \; + \; + (f-1)^2 \; + (f-1)(f-2) \; + \; + (f-1) \; + (f-1)^2 \; + \; + (f-1)^2 (f-2) \; \Big]$$

$$\langle R_{00}^2 \rangle = 2N + 2u \Big[\; 2 \; + \; + 2(2f-3) \; + \; + 2(f-1)(f-2) \; (\; + \;) \; + \; + 2(f-1)^2 (f-2) \; + \; + (f-1)^2 \; \Big]$$

$$\langle R_{11}^2 \rangle = 4N + 2u \Big[\; 4 \; + 3 \; + 6(f-2) \; + \; + 2 \; + 4(f-2) \; + \; + 2(f-1)(f-2) \; + 2(f-1)^2 \; + \; + \; + 2(f-2) \; + \; + 2(f-1)(f-2) \; + \; + 2(f-1)(f-2)^2 \; + \; + (f-2)^2 \; \Big]$$

Appendix B

Forms and values of the diagrams:

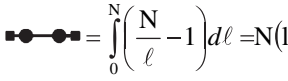

$$= \int_0^{\mathrm{N}} \left(\frac{\mathrm{N}}{\ell} - 1 \right) d\ell = \mathrm{N}(\ln N - 1)$$

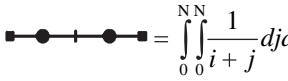

$$= \int_0^{\mathrm{N}} \int_0^{\mathrm{N}} \frac{1}{i+j} djdi = 2\mathrm{N}\ln 2$$

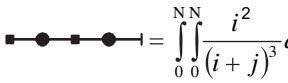

$$= \int_0^{\mathrm{N}} \int_0^{\mathrm{N}} \frac{i^2}{(i+j)^3} djdi = \mathrm{N}\left(\ln 2 - \frac{1}{4} \right)$$

$$= \int_0^{\mathrm{N}} \int_0^{\mathrm{N}} \frac{1}{i+j+\mathrm{N}} djdi = \mathrm{N}(3\ln 3 - 4\ln 2)$$

$$= \int_0^{\mathrm{N}} \int_0^{\mathrm{N}} \frac{(i+\mathrm{N})^2}{(i+j+\mathrm{N})^3} djdi = \mathrm{N}\left(\ln 3 - \ln 2 - \frac{1}{12} \right)$$

$$= \int_0^{\mathrm{N}} \int_0^{\mathrm{N}} \frac{i^2}{(i+j+\mathrm{N})^3} djdi = \mathrm{N}\left(2\ln 3 - 3\ln 2 - \frac{1}{12} \right)$$

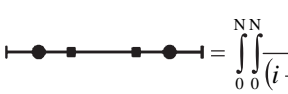

$$= \int_0^{\mathrm{N}} \int_0^{\mathrm{N}} \frac{\mathrm{N}^2}{(i+j+\mathrm{N})^3} djdi = \mathrm{N}\left(\frac{1}{6} \right)$$

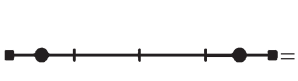

$$= \int_0^{\mathrm{N}} \int_0^{\mathrm{N}} \frac{1}{i+j+2\mathrm{N}} djdi = 2\mathrm{N}(5\ln 2 - 3\ln 3)$$

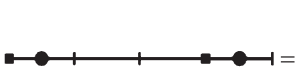

$$= \int_0^{\mathrm{N}} \int_0^{\mathrm{N}} \frac{(i+2\mathrm{N})^2}{(i+j+2\mathrm{N})^3} djdi = \mathrm{N}\left(2\ln 2 - \ln 3 - \frac{1}{24} \right)$$

$$= \int_0^{\mathrm{N}} \int_0^{\mathrm{N}} \frac{(i+\mathrm{N})^2}{(i+j+2\mathrm{N})^3} djdi = \mathrm{N}\left(5\ln 2 - 3\ln 3 - \frac{1}{12} \right)$$

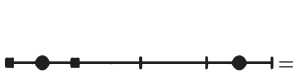

$$= \int_0^{\mathrm{N}} \int_0^{\mathrm{N}} \frac{i^2}{(i+j+2\mathrm{N})^3} djdi = \mathrm{N}\left(8\ln 2 - 5\ln 3 - \frac{1}{24} \right)$$

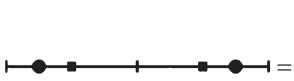

$$= \int_0^{\mathrm{N}} \int_0^{\mathrm{N}} \frac{(2\mathrm{N})^2}{(i+j+2\mathrm{N})^3} djdi = \mathrm{N}\left(\frac{1}{6} \right)$$

$$= \int_0^{\mathrm{N}} \int_0^{\mathrm{N}} \frac{\mathrm{N}^2}{(i+j+2\mathrm{N})^3} djdi = \mathrm{N}\left(\frac{1}{24} \right)$$

Appendix C

Analytical expressions of the mean end-to-end square distances of all possible branches $\langle r_0^2 \rangle$, $\langle r_1^2 \rangle$ and $\langle R_{01}^2 \rangle$ and the respective expressions for the diameters of the zeroth generation $\langle R_{00}^2 \rangle$ and the whole dendritic chain $\langle R_{11}^2 \rangle$. The diameter of star polymer chain $\langle D_{\mathrm{star}}^2 \rangle$ and the mean end-to-end square distance of star polymer arm $\langle R_{\mathrm{star}}^2 \rangle$with length N have been calculated from Ref. [24].

$$\langle r_0^2 \rangle = N\left\{ 1 + u\left[2\ln N + f^3 \frac{1}{12} + f^2\left(4\ln 3 - 6\ln 2 - \frac{1}{12} \right) + f\left(16\ln 2 - 8\ln 3 - \frac{13}{12} \right) - 10\ln 2 + 4\ln 3 - \frac{11}{12} \right] \right\}$$

$$\langle r_1^2 \rangle = N\left\{ 1 + u\left[2\ln N + f^2\left(16\ln 2 - 10\ln 3 - \frac{1}{12} \right) + f\left(24\ln 3 - 36\ln 2 - \frac{1}{2} \right) - 14\ln 3 + 20\ln 2 - \frac{17}{12} \right] \right\}$$

$$\langle R_{01}^2 \rangle = 2N\left\{1+u\left[2\ln N + f^3\frac{1}{24} + f^2\left(2\ln 2 - \ln 3 - \frac{1}{6}\right) + f\left(3\ln 3 - 2\ln 2 - \frac{19}{24}\right) - 2\ln 3 - \frac{7}{12}\right]\right\}$$

$$\langle R_{00}^2 \rangle = 2N\left\{1+u\left[2\ln N + f^3\frac{1}{12} + f^2\left(4\ln 3 - 6\ln 2\right) + f\left(20\ln 2 - 10\ln 3 - \frac{19}{12}\right) + 6\ln 3 - 14\ln 2\right]\right\}$$

$$\langle R_{11}^2 \rangle = 4N\left\{1+u\left[2\ln N + f^3\frac{1}{24} + f^2\left(2\ln 2 - \ln 3 - \frac{1}{8}\right) + f\left(4\ln 3 - 3\ln 2 - \frac{9}{8}\right) + 2\ln 2 - 4\ln 3 + \frac{5}{12}\right]\right\}$$

$$\langle R_{\mathrm{star}}^2 \rangle = N\left\{1+u\left[2\ln N + f\left(2\ln 2 - \frac{1}{2}\right) - 2\ln 2 - \frac{3}{2}\right]\right\}$$

$$\langle D_{\mathrm{star}}^2 \rangle = 2N\left(1+\mathrm{u}\left(2\ln N + f\left(2\ln 2 - \frac{1}{2}\right) - 2\ln 2 - 1\right)\right)$$

References

[1] Frechet JM, Tomalia DA. Dendrimers and other dendritic polymers. Wiley Series in Polymer Science; 2001.
[2] Editorial. Prog Polym Sci 2005;30:217.
[3] Gauthier M, Moller M. Macromolecules 1991;24:4548.
[4] Tomalia DA, Hedstrand DM, Ferritto MS. Macromolecules 1991;24: 1435.
[5] Gauthier M, Tichagwa L, Downey J, Gao S. Macromolecules 1996;29: 519.
[6] Grubbs RB, Hawker CJ, Dao J, Frechet JM. Angew Chem Int Ed Engl 1997;36:270.
[7] Knauss DM, Al-Muallem HA. J Polym Sci Part A Polym Chem 2001;39: 152.
[8] Knauss DM, Huang T. Macromolecules 2002;35:2055.
[9] Six JL, Gnanou Y. Macromol Symp 1995;95:137.
[10] Angot S, Taton D, Gnanou Y. Macromolecules 2000;33:5418.
[11] Knauss DM, Al-Muallem HA. J Polym Sci Part A Polym Chem 2000;38: 4289.
[12] Al-Muallem HA, Knauss DM. J Polym Sci Part A Polym Chem 2001;39: 3547.
[13] Knauss DM, Al-Muallem HA, Huang T, Wu D. Macromolecules 2000; 33:3557.
[14] Chalari I, Hadjichristidis N. J Polym Sci Part A Polym Chem 2002;40: 1519.
[15] Murat M, Grest G. Macromolecules 1996;29:1278.
[16] Chen Z, Cui S. Macromolecules 1996;29:7943.
[17] Lyulin A, Davies G, Adolf D. Macromolecules 2000;33:6899.
[18] Mansfield M, Jeong M. Macromolecules 2002;35:9794.
[19] Ballauff M, Likos C. Angew Chem Int Ed 2004;43:2998.
[20] Rathgeber S, Pakula T, Urban V. J Chem Phys 2004;121:3840.
[21] de Gennes PG, Hervet H. J Phys Lett 1983;44:L351.
[22] Biswas P, Cherayil B. J Chem Phys 1994;100:3201.
[23] Ganazzoli F, Ferla R, Terragni G. Macromolecules 2000;33:6611.
[24] Vlahos CH, Kosmas MK. Polymer 1984;25:1607.
[25] Rubio A, Brea P, Freire J, Kosmas M, Vlahos C. Macromolecules 2000; 33:207.
[26] Kosmas M, Vlahos C, Avgeropoulos A. J Chem Phys 2006;125:094908.
[27] Theodorakis PE, Avgeropoulos A, Freire J, Kosmas M, Vlahos C. Macromolecules 2006;39:4235.
[28] Uhrig D, Mays JW. J Polym Sci Part A Polym Chem 2005;43: 6179.
[29] Iatrou H, Hadjichristidis N. Macromolecules 1992;25:4649.
[30] Ma JJ, Bronn WR, Silver SF. Polym Prepr (Am Chem Soc Div Polym Chem) 1994;35:572.
[31] Cohen RE, Willfong DE. Macromolecules 1982;15:370.
[32] Freire J, Pla J, Rey A, Prats R. Macromolecules 1986;19:453.
[33] Wittkop M, Kreitmeier S, Goritz D. J Chem Phys 1996;104:3373.
[34] Brandrup J, Immergut EH, Grulke EA. Polymer handbook. 4th ed. Wiley-Interscience; 1999 [chapter VI].